JOURNAL OF CATALYSIS 114, 71–89 (1988)

Catalytic Cracking Studies and Characterization of Steamed Y and LZ-210 Zeolites

REGIS J. PELLET, C. SCOTT BLACKWELL, AND JULE A. RABO

Union Carbide Corporation, Tarrytown, New York 10591

Received November 18, 1987; revised May 26, 1988

Catalytic cracking catalysts prepared using Y zeolite crystals which have been silicon enriched by treatment with ammonium fluorosilicate solution show substantially superior crystal retention upon exposure to severe hydrothermal treatments, relative to similarly treated Y-zeolite-based catalysts. The silicon-enriched Y-based catalysts, following hydrothermal pretreatment, also show superior activity retention and higher gasoline selectivity relative to Y-zeolite-based catalysts. The study of steamed Y and the silicon-enriched Y product by solid-state MAS NMR shows that upon steaming the silicon-enriched zeolite displays superior retention of the framework structure relative to Y, and that the Y product shows not only aluminum loss but also significant silicon loss from the crystal framework, contributing to deterioration of the crystal. Thermometric titrations of Y zeolites, following exposure to steam treatments of increasing severity, indicates that upon severe steam treatment the strong acid character typical of stabilized Y is greatly reduced while a substantial concentration of milder acid sites is formed, similar in acid strength to amorphous silica–alumina gel. These data are interpreted on the basis that upon steaming amorphous alumina and silica–alumina phases are formed, occluded in the zeolite crystal, and that the occluded amorphous, acidic debris adversely affects cracking selectivity to produce gasoline.

INTRODUCTION

The preparation of framework silicon-enriched Y zeolites, called LZ-210, at silica–alumina ratios of 6 and above has been reported using aqueous ammonium fluorosilicate solutions as silicon-enriching agents (*1*). The LZ-210 enrichment process permits the variation of Y framework composition while maintaining high crystal integrity. Framework silicon enrichment has been shown to dramatically enhance thermal and hydrothermal stability of the Y crystal (*2*). Cracking catalysts prepared from LZ-210 zeolites exhibit enhanced selectivity to high octane gasoline (*3*).

In commercial use the FCC catalyst is exposed to severe hydrothermal environments in the regenerator section of the FCC unit. Under these conditions significant crystal degradation and dealumination of the zeolite crystal framework are known to occur. By using rare-earth-exchanged forms of Y, a significant portion of zeolite framework can be maintained. However, in H–Y-type zeolites most of the framework aluminum is converted to an amorphous alumina-containing phase, occluded in the zeolite crystal structure as extra framework debris. The amount of aluminum remaining in framework positions depends upon steaming severity and rare-earth cation content.

Pine and co-workers (*4*) have discussed the significance of framework aluminum content (evaluated from zeolite crystal unit cell size) on cracking performance for a series of steam-stabilized and rare-earth-exchanged Y-based cracking catalysts. In their work, using steam-deactivated catalysts, MAT cracking activity was found to correlate directly with the Y zeolite unit cell size of the steam-deactivated catalysts. Cracking selectivity and product gasoline octane correlated inversely with this parameter. These workers concluded that the Y catalyst performance was related to the Y crystal framework aluminum content; the

0021-9517/88 $3.00

TABLE 1

Physical and Chemical Properties of Zeolites

Zeolite base	SiO_2/Al_2O_3[e]	Na_2O (wt%)	$(NH_4)_2O_2$ (wt%)	SiO_2 (wt%)	Al_2O_3 (wt%)	a_0[a]
Y-82[b]	5.8	0.17	4.04	73.7	21.7	24.55
Y-82[b]	6.2	0.14	4.3	74.8	20.6	24.57
LZ-210[c]	7.4	1.28	6.3	74.9	17.1	24.56
NH_4–LZ-210[d]	7.4	0.26	7.7	75.5	16.9	24.66
LZ-210[c]	8.3	1.05	5.64	76.4	15.7	24.55
NH_4–LZ-210[d]	8.3	0.05	7.6	75.3	15.3	24.58
LZ-210[c]	11.0	0.39	6.1	79.5	12.3	24.46
NH_4–LZ-210[d]	11.7	0.05	5.4	83.4	12.2	24.42
LZ-210[c]	16.7	1.31	3.06	85.6	8.7	24.42
LZ-210[c]	19.5	0.18	3.7	88.0	7.65	24.46

[a] Unit cell constant, as determined from X-ray diffraction data.
[b] Steam-stabilized and NH_4-exchanged Y.
[c] Chemically silicon-substituted Y, LZ-210.
[d] Ammonium-exchanged LZ-210.
[e] Calculated from chemical analysis.

latter was estimated from Y crystal unit cell size. Their study, however, was limited to catalysts prepared from Y zeolites including aluminum-extracted products with initial silica-to-alumina ratios ranging from 5.0 to 6.5. Since the total aluminum content (both framework and nonframework) was therefore fixed between 45 and 55 aluminum atoms per Y zeolite unit cell, their study was lacking the data base to independently examine the influence of nonframework aluminum content on FCC performance.

Using LZ-210 zeolites with varying silica-to-alumina ratios large variations in zeolitic framework aluminum content became possible for the nonsteamed materials. Variations ranging from 45 down to 17 aluminum atoms per unit cell are reported in this and in previous reports (*2, 3*). The total aluminum content of the fresh zeolite base can be controlled by the silicon enrichment process. The ratios of framework versus nonframework aluminum content of steamed LZ-210 zeolites can be controlled by the choice of steaming severity. Therefore, it is now possible to vary independently in the Y zeolite crystal lattice the framework and nonframework aluminum contents by the choice of LZ-210 silica-to-alumina ratio and severity of steam treatment. This study describes the catalytic properties of steam-treated NH_4Y, (Y-82) and NH_4–LZ-210 zeolites in catalytic cracking using MAT experiments. In addition, in the second part of the paper, physical and chemical characterization is given, using solid-state NMR, electron microscopy, porosimetry, and thermometric titration to characterize untreated and steamed NH_4Y and NH_4–LZ-210 zeolites.

EXPERIMENTAL

Catalyst Preparation and Evaluation

The properties of all zeolites used in the present study are summarized in Table 1. The steam-treated and ammonium-exchanged Y was obtained from Union Carbide Corporation as Y-82. All LZ-210 products were prepared by treatment of ammonium Y (silica/alumina ratio of 5.0) with ammonium hexafluorosilicate (AFS) solutions as described in the literature (*1*). The silica/alumina ratio of the LZ-210 product was controlled by careful control of the

TABLE 2

FCC Catalyst[a] Properties following Steam Deactivation at 840°C for 17 h in 23% Steam/Air Mixture

Zeolite base	SiO_2/Al_2O_3	Fresh catalyst zeolite content (%)[b]	Steamed catalyst crystal content (%)[c]	Unit cell size[d] (Å)
Y-82	5.8	14.8	2.7	24.21
Y-82	6.2	14.8	3.6	24.23
LZ-210	7.4	14.8	5.0	24.30
NH_4–LZ-210	7.4	14.6	5.0	24.28
LZ-210	8.3	15.0	4.0	24.24
NH_4–LZ-210	8.3	14.9	6.1	24.26
LZ-210	11.0	15.2	8.5	24.28
NH_4–LZ-210	11.7	14.6	8.8	24.27
LZ-210	16.7	15.2	6.5	24.27
LZ-210	19.5	15.2	11.0	24.30

[a] All catalysts were prepared to contain 15% zeolite and 85% alumina matrix and binder.

[b] Zeolite content of the finished catalyst was determined from chemical analysis of its silica content.

[c] Percentage crystal content remaining in catalyst following destructive steaming as determined by X-ray diffraction peak area retention, relative to reference, unsteamed NH_4Y[b].

[d] Determined from X-ray diffraction data obtained from the steam-deactivated catalyst.

amount of AFS reagent used. In addition, several of the LZ-210 products were subjected to subsequent ammonium exchange to reduce their soda content as noted in Table 1.

The experimental catalyst formulations prepared from these zeolites are described in Table 2. In order to obtain MAT FCC performance data, all zeolite species were formulated into catalysts containing 15% zeolite, 65% boehmite alumina matrix, and 20% peptized alumina binder. Typically, the zeolite was mixed with matrix in a Hobart mixer to which the peptized alumina was added. This composite was then extruded to form $\frac{1}{16}$-in. extrudates, dried at 100°C, and calcined in dry air at 500°C in order to set the binder. In order to simulate the degradive environment of the FCC regenerator and to observe characteristic differences in zeolites with varying hydrothermal behaviors, all catalysts were steam deactivated under fairly severe conditions. Thus, calcined catalyst extrudates were brought to 750°C rapidly in static air. Subsequently, a 23% steam/air mixture was passed over the catalysts and the temperature was brought to 840°C and maintained there for 17 h. Following steam treatment each deactivated catalyst was analyzed for X-ray crystallinity and unit cell size according to ASTM procedure D3942-85 or ground to 60/100 mesh particles prior to catalytic testing. All catalysts were next evaluated for performance in FCC applications by the microactivity test procedure defined by the ASTM method D-3907. All catalysts were evaluated at 900°F, at a catalyst-to-oil ratio of 3.0 and at a weight hourly space velocity of 16. All runs were carried out in reactors whose configurations were equivalent to that described in ASTM D-3907. All products were collected and analyzed. Product analysis was used to calculate conversion and product selectivities and yields.

NMR Experiments

Selected samples were run on a Bruker MSL-400 solid-state and high-resolution multinuclear NMR spectrometer operating at a magnetic field of 9.4 T (79.494 MHz for ^{29}Si, 104.262 MHz for ^{27}Al). Some Si cross polarization was done at 4.7 T (39.74 MHz) using a Bruker CXP-200. Typical experiments performed were fully relaxed ^{29}Si and ^{27}Al Bloch decays, (^1H–^{29}Si) CP-MAS and (^1H–^{27}Al) CP-MAS. Quantitative ^{29}Si NMR was performed using 2-μs pulses followed by a 90-s recycle delay, sweep width of 20 kHz, and 8K data table. Quantitative ^{27}Al NMR was done with 1-μs pulses, 125-kHz sweep width, 16-μs deadtime, 8192 data points, and a 2-s recycle time. All samples were run with Bruker DB (double bearing) tunable broadband CP-MAS probes specially selected to have Si-free and Al-free spectral backgrounds; appropriate rotors were used to minimize background problems. The chemical shifts observed were referenced to external standards. For ^{29}Si NMR, external TMS (tetramethylsilane) was used to establish $\delta = 0$ ppm; for

^{27}Al NMR a 1 *M* $Al(NO_3)_3$ aqueous solution was used to set for $\delta = 0$ ppm. The chemical shifts for ^{29}Si NMR should not differ in any substantial manner whether a 4.7- or 9.4-T experiment is done. However, ^{27}Al NMR shifts are subject to second-order quadrupole broadening, which can result in apparent shifts for the observed values of δ. If the change is due to a quadrupolar effect, the value for δ determined for the 9.4-T spectrum will always be higher (more deshielded) than that found at 4.7 T. This is the second-order quadrupolar shift effect and it dictates that special care must be taken in comparing data obtained at 4.7 T with that determined at 9.4 T.

RESULTS AND DISCUSSIONS

Catalytic Cracking (MAT) Studies with H–Y and with H–LZ-210 Zeolites

The present study examines effects of the zeolite framework aluminum as well as the nonframework aluminum contents on catalytic cracking performance. The zeolite samples were prepared with the intent to generate by steam treatment a broad range of nonframework aluminum contents, with relatively smaller variations in framework aluminum content. To this end, zeolite Y derivatives with a broad range of silica-to-alumina ratios were synthesized, ranging from 5.8 for steam-stabilized NH_4Y up to 19.5 using LZ-210 products. Each zeolite composition tested was prepared in low-soda (0.05 to 1.3% Na_2O) and NH_4-exchanged form. Properties of the Y and LZ-210 zeolites studied are summarized in Table 1.

In order to obtain MAT FCC performance data, all zeolite species were formulated into catalysts containing 15% zeolite and 65% boehmite alumina matrix and 20% peptized alumina binder. Subsequently, they were steam deactivated at 840°C in 23% steam/air mixture for 17 h to simulate the destructive environment of the FCC regenerator. It should be noted that the steaming condition selected for this study is fairly severe. It was chosen to provide an opportunity to observe characteristic differences in cracking performance of zeolites with varying hydrothermal behavior and to observe the catalytic behavior of zeolite catalysts rich in extra-framework aluminum. The properties of the steam deactivated catalysts are summarized in Table 2. Comparison with the data in Table 1 shows that the steam treatment has significantly reduced the unit cell size of both Y and LZ-210 crystals in the catalysts, indicating significant dealumination of the zeolite frameworks. Extensive zeolite framework dealumination and a corresponding drop in crystal unit cell size is expected for both Y and LZ-210 species at the low metal-cation contents used. Final unit cell sizes varied from 24.21 to 24.30 Å. Crystallinity retention, as calculated from X-ray peak areas, was significantly reduced for several samples. Significantly, the amount of crystallinity retained in these steamed catalysts is inversely related to the amount of initial framework aluminum present in the starting zeolites as shown in Fig. 1. Here, the crystal content of the steam-deactivated cata-

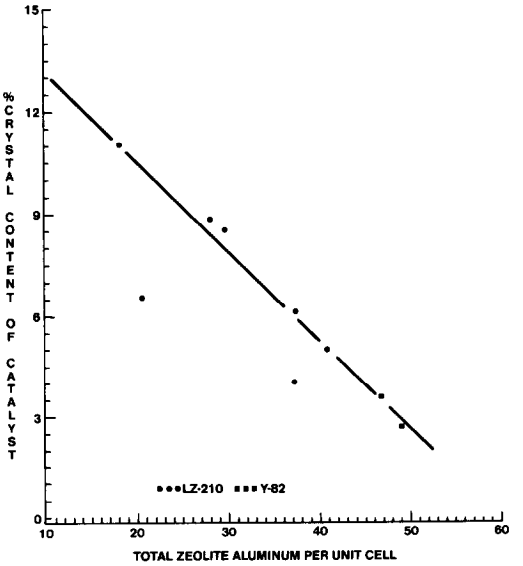

FIG. 1. Percentage crystal content retained in steamed catalysts as a function of the total zeolite aluminum content.

lysts are plotted against their initial framework aluminum contents, given in terms of aluminum atoms per unit cell. The crystal contents are calculated relative to unsteamed reference NH_4Y. The steam-stabilized and subsequently NH_4-exchanged NH_4Y-based catalysts with the highest zeolite aluminum content (45 to 49 Al/uc) exhibit only 2.7 and 3.6% crystal content, or about 18 to 24% crystal retention relative to the unsteamed reference NH_4Y. The LZ-210-based catalysts exhibit as much as 11% crystal content after steaming, representing over 70% crystal retention of the original 15% zeolite in the catalyst.

Correlations among Catalyst Activity, Selectivity, and the Silica-to-Alumina Ratio of Zeolites

All steam-deactivated catalysts described in Table 2 were evaluated for FCC cracking performance in the standard microactivity test (MAT) as defined by the ASTM method (*5*). The activity data obtained from these tests are summarized in Table 3 and in Fig. 2 where percentage MAT conversion is plotted as a function of total zeolite aluminum content, including both framework and nonframework, per unit cell. The data in Fig. 2 show that the activity of the steam-deactivated catalysts

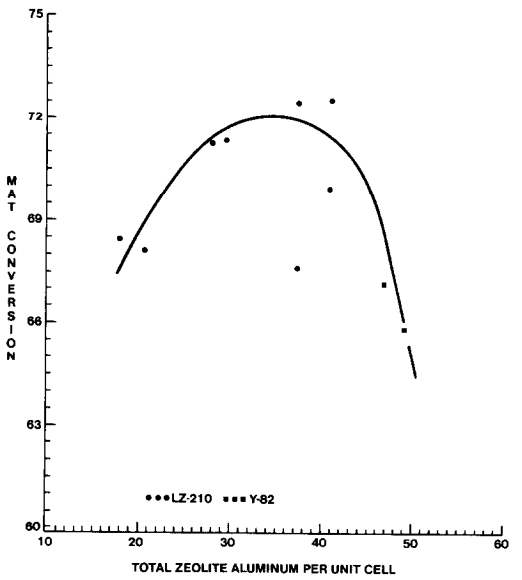

FIG. 2. Percentage MAT conversion plotted as a function of total zeolite aluminum content.

TABLE 3

FCC Cracking Activity Trends

Zeolite base	SiO_2/Al_2O_3	Steamed catalyst crystal content[a]	Total aluminum per unit cell[b]	Conversion[c]	Specific conversion[d]
Y-82	5.8	2.7	49.2	65.8	24.4
Y-82	6.2	3.6	46.8	67.1	18.6
LZ-210	7.4	5.0	40.9	72.5	14.5
NH_4–LZ-210	7.4	5.0	40.9	69.9	14.0
LZ-210	8.3	4.0	37.3	67.6	16.9
NH_4–LZ-210	8.3	6.1	37.3	72.4	11.8
LZ-210	11.0	8.5	29.5	71.3	8.4
NH_4–LZ-210	11.7	8.8	28.0	71.2	8.1
LZ-210	16.7	6.5	20.5	68.1	10.5
LZ-210	19.5	11.0	17.9	68.4	6.2

[a] Percentage crystal content remaining in catalyst following destructive steaming as determined by X-ray diffraction peak area retention, relative to reference, unsteamed NH_4Y.

[b] Calculated from the chemical analysis of the unsteamed zeolite base (see Table 1).

[c] Percentage conversion determined by the microactivity test method (MAT) as defined by ASTM. Percentage conversions given are an average of at least three MAT runs each achieving mass balance greater than 95%.

[d] Specific conversion is the MAT conversion divided by percentage crystal retention of the steamed catalyst.

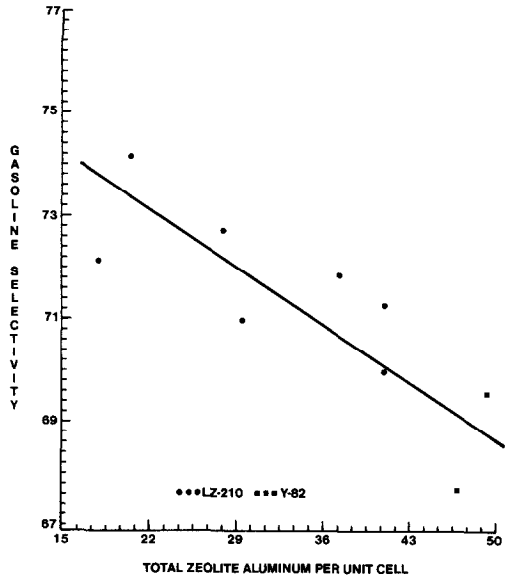

FIG. 3. The decrease in gasoline selectivity with increasing zeolite aluminum content.

goes through a maximum at about 40 aluminum atoms per unit cell (a silica/alumina ratio of 7–8). The data also show that following steaming all LZ-210 zeolites have higher cracking activity relative to steam-stabilized Y (Y-82).

Parallel with the MAT activity tests, gasoline selectivities (gasoline yield/conversion) were also determined from the same data base. In order to compare the gasoline selectivity of different catalysts in a meaningful way one must use data obtained at a comparable conversion. With this objective in mind only those MAT runs which fell within ±3% of 70% conversion were used for this comparison. Furthermore, each conversion point was based on the average value of at least three parallel MAT runs, each achieving a mass balance greater than 95%. Data meeting these criteria under constant MAT conditions are summarized in Table 5. The data in Table 5 and Fig. 3 show a strong inverse relationship between the aluminum content of the starting zeolite (total aluminum) and gasoline selectivity. Clearly, the gasoline selectivity increases steadily with increased silicon enrichment in the Y crystal, ranging from 67.9% for steamed NH_4Y to about 74.3% for LZ-210 with a silica-to-alumina ratio of 16.7; see Table 5 and Fig. 3. It is worth noting that the conversions for the catalysts of highest and lowest gasoline selectivities were similar (Table 3) and that the selectivity increase does not coincide with a trend to higher activity; see Figs. 2 and 3 and Tables 3 and 5.

Effect of Crystallinity on Catalytic Activity

The activity and selectivity correlations given above for catalysts with Y crystals of varying silica-to-alumina ratios can be further analyzed by attempting to correlate catalyst activity and selectivity with structural and chemical characteristics of the zeolite component of the steamed catalyst. One of these characteristics is catalyst crystal content following steam treatment. Thus, further insight into the effect of zeolite crystal retention on cracking activity may be obtained by defining a specific or intrinsic activity parameter:

$$\text{Specific conversion} = \text{MAT\% conversion}/\text{\% crystal content}. \quad (1)$$

In this equation the crystal content is given for the steam-deactivated catalysts as the X-ray peak area retained by the zeolite containing catalyst relative to unsteamed reference ammonium Y zeolite. Thus specific conversion is a measure of activity per unit amount of crystal remaining, following steam treatment. In Fig. 4, specific conversions for the LZ-210- and Y-82-based catalyst series are plotted against total (initial) zeolite aluminum content. According to this correlation, there is a direct, linear relationship between specific conversion and total zeolite aluminum content. Catalysts based on Y of high total aluminum content exhibit higher specific conversion than the silicon-enriched LZ-210-type catalysts. Furthermore, within the LZ-210 series, the

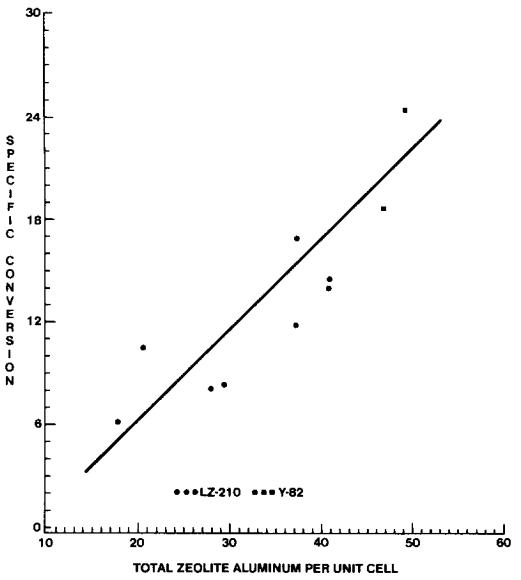

FIG. 4. A plot of specific conversion as a function of total zeolite aluminum.

specific conversion is directly related to the total aluminum content of the starting zeolite.

In order to interpret these observations one must note that as a result of the relatively severe steam pretreatment, the aluminum-rich zeolites, particularly the Y-82-based catalysts, lost most of their Y crystallinity. In addition, both Y and LZ-210 zeolites lost most of their framework aluminum content, as indicated by the low value of the crystal lattice constants. Consequently, the usually dominant zeolitic acidity which is related to the framework aluminum has been reduced to a small fraction of its original value. In these circumstances, considering the absence of rare earth cations, the formation of amorphous silica–alumina phases is expected. These phases will be formed from collapsed sections of the H–Y zeolite. In addition, it is expected that even the remaining crystal phases will contain significant amounts of amorphous material as a result of the extensive framework dealumination. Thus, the correlation between specific conversion and starting zeolite aluminum content can be interpreted on the basis that both the surviving zeolite crystals and the amorphous silica–alumina debris contribute to catalytic activity. Furthermore, the high specific conversion obtained with the catalyst of lowest zeolite crystal retention and highest amorphous debris phase indicates that below a certain minimum framework aluminum content and retained crystallinity, the amorphous phase will dominate catalytic performance.

Effect of Aluminum Distribution on Catalytic Activity and Selectivity

Since the strong acid character of Y zeolite is related to framework aluminum content, relationships between framework and nonframework aluminum content and catalytic performance are of great interest. The nonframework aluminum content in the present series of catalysts is estimated as the difference between the total aluminum content given by chemical analysis and the framework aluminum content calculated from the unit cell size of the zeolite. The relationship between zeolite unit cell size and framework aluminum content has been described earlier in the literature. Originally this relationship was determined by Breck and Flanigen (*7*) using X and Y zeolites in the synthesized sodium form:

$$\text{Framework aluminum per unit cell} = 115.2(a_0 - 24.191). \quad (2)$$

This relationship was applied only for Y zeolites with silica/alumina ratios of 5 and below (i.e., greater than 55 aluminum atoms per unit cell) for hydrated, as-synthesized zeolites. The use of this equation is, however, not appropriate in a quantitative sense for steamed or chemically modified Y zeolites. Here, upon steaming, both the lattice defects and the occlusion of cationic aluminum oxide clusters in the sodalite cages may affect the lattice constant to an unknown degree. More recently, Lunsford and co-workers (*8*) have proposed a similar relationship for chemically treated and

TABLE 4

Zeolite Aluminum Distribution of Steam-Deactivated Catalysts (840°C, 17 h, 23% Steam/Air Mixture)

Zeolite base	SiO_2/Al_2O_3	Aluminum atoms per zeolite unit cell			
		Total[a]	Framework[b]	Framework[c]	Nonframework[d]
Y-82	5.8	49.2	0.0	−3.0	49.2
Y-82	6.2	46.8	1.5	−0.9	45.3
LZ-210	7.4	40.9	9.2	6.6	31.7
NH_4–LZ-210	7.4	40.9	7.0	4.5	33.9
LZ-210	8.3	37.3	2.5	0.2	34.8
NH_4–LZ-210	8.3	37.3	4.8	2.4	32.5
LZ-210	11.0	29.5	7.0	4.5	22.5
NH_4–LZ-210	11.7	28.0	5.9	3.4	22.1
LZ-210	16.7	20.5	5.9	3.4	14.6
LZ-210	19.5	17.9	9.2	6.6	8.7

[a] Calculated from the chemical analysis of the unsteamed zeolite (see Table 1).

[b] Framework aluminum content of steamed zeolite catalysts estimated from the unit cell size (determined by XRD) and using the Breck–Flanigen equation: framework Al = $115.2(a_0 - 24.191)$.

[c] The framework aluminum content of steamed zeolites estimated from unit cell size (determined by XRD) and correlation from J. R. Sohn *et al.* (*Zeolites* **6**, 225 (1986)): framework Al = $107.1(a_0 - 24.238)$.

[d] Nonframework aluminum content of steamed zeolite catalysts was estimated as the difference between the total zeolite aluminum content determined by chemical analysis and the framework aluminum content estimated from the Breck–Flanigen equation.

steamed Y zeolites, presumably containing 0 to 50 framework aluminum atoms per unit cell. These workers used NMR as a presumably quantitative tool to independently determine framework aluminum content:

$$\text{Framework aluminum per unit cell} = 107.1(a_0 - 24.238). \quad (3)$$

While both equations are similar, the work of Lunsford is significant in the present consideration because it intends to provide an estimate of framework aluminum content for steamed H–Y materials.

In the present study, both equations have been used to estimate the amount of framework aluminum in the series of steam-deactivated catalysts, using the unit cell constants reported in Table 2. Results of this exercise are presented in Table 4. Comparison of results indicates that while both equations indicated the same trends, the Lunsford equation predicts negative framework aluminum contents for severely steamed materials. Clearly, neither equation is applicable to yield precise values for the framework aluminum content of severely steamed Y or LZ-210 products. Both relationships are, however, adequate to indicate the trend and the range of aluminum depletion from the zeolite framework. By calculation of the framework aluminum from the two equations and with the total aluminum determined by chemical analysis, the relationships between framework and nonframework aluminum and catalytic performance were examined.

The data in Table 4 show that following steam treatment at 840°C for 17 h most of the framework aluminum has been removed from the zeolite crystal lattice. Along with the dealumination of the zeolite crystal the severe steaming results in the collapse of substantial fractions of the zeolite crystal. Both the alumina removed from the zeolite lattice and the amorphous silica–alumina formed upon crystal collapse have

potential contributions to cracking activity. Therefore, correlations are presented for the contribution of framework aluminum, and of nonframework aluminum and amorphous silica–alumina phase, on cracking performance.

As mentioned above, Pine and co-workers have shown that FCC gasoline octane and gas product olefinicity vary inversely with the unit cell size of steam-deactivated Y catalysts. Table 5 presents product quality information obtained in MAT evaluation of the present set of catalysts. While the amount of product generated in MAT experiments does not permit determination of gasoline octane rating by engine octane methods, it is possible to estimate relative gasoline octane ratings from the olefinicity of the cracked products. Thus Table 5 presents data for the propylene content of the C_3 gas make obtained over the catalysts studied here. Since conversion is known to effect catalytic selectivity, it is essential that selectivity comparisons between catalysts be made at or near equivalent conversions. Thus the olefinicity data presented in Table 5 were obtained from MAT runs within 3% of 70% conversion. The correlations of C_3 olefinicity with framework and nonframework aluminum contents are presented graphically in Figs. 5 and 6, respectively. It can be seen that a fairly good cor-

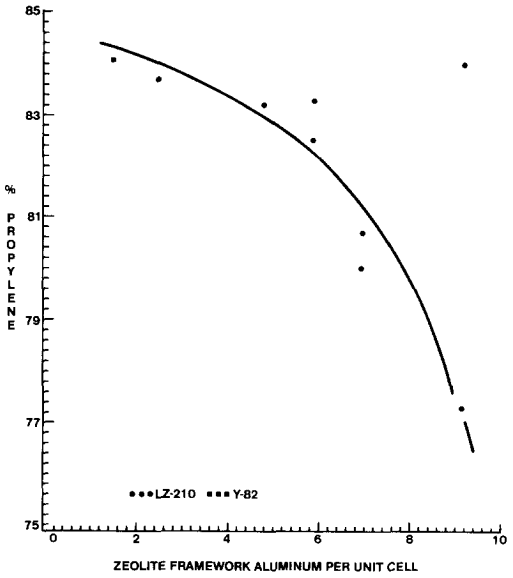

FIG. 5. The correlation of C_3 olefinicity with zeolite framework aluminum content following steam treatment.

TABLE 5

Gasoline and Propylene Selectivities at 70% MAT Conversion

Zeolite base		Framework Al per unit cell[a]	Nonframework Al per unit cell[b]	Gasoline selectivity[c]	% Propylene in C_3 gas make[d]
Type	SiO_2/Al_2O_3				
Y-82	6.2	1.5	45.3	67.9	84.1
LZ-210	7.4	9.2	31.7	71.4	84.0
NH_4–LZ-210	7.4	7.0	33.9	70.1	80.0
LZ-210	8.3	2.5	34.8	75.7	83.7
NH_4–LZ-210	8.3	4.8	32.5	72.0	83.2
LZ-210	11.0	7.0	22.5	71.1	80.7
NH_4–LZ-210	11.7	5.9	22.1	72.9	82.5
LZ-210	16.7	5.9	14.6	74.3	83.3
LZ-210	19.5	9.2	8.7	72.3	77.3

[a] Framework aluminum content of steamed zeolite catalysts estimated from the unit cell size (determined by XRD) and using the Breck–Flanigen equation: framework Al = $115.2(a_0 - 24.191)$.

[b] Nonframework aluminum content of steamed zeolite catalysts was estimated as the difference between the total zeolite aluminum content determined by chemical analysis and the framework aluminum content estimated from the Breck–Flanigen equation.

[c] Gasoline selectivity = (gasoline yield) (% conversion) × 100 for conversion = 70 ± 3%.

[d] Actual propylene content of C_3 gas make at 70 ± 3% conversion.

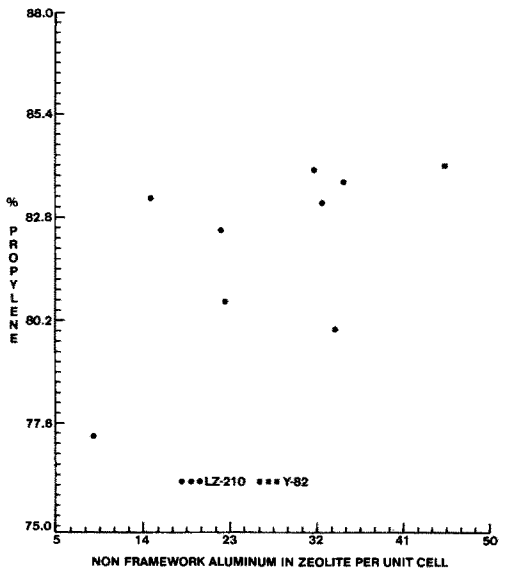

FIG. 6. A lack of correlation of C_3 olefinicity with the zeolite nonframework aluminum content following steam treatment.

relation exists with framework aluminum, in agreement with previously published results (*4*). Interestingly, no apparent correlation can be found between C_3 olefin content and nonframework aluminum, even though, here again, the nonframework aluminum term includes not only the alumina formed upon framework hydrolysis but also the amorphous phases formed from collapsed crystals. The data in Fig. 5 indicate that as the amount of framework aluminum decreases, the olefinicity of the C_3 products increases. Presumably similar trends occur in the gasoline range products, indicating an increase in gasoline octane with declining zeolitic framework aluminum content. The increased product olefinicity and gasoline octane observed in previous reports (*4*) has been attributed to a reduction of the hydrogen transfer reactions catalyzed by strong acid sites, associated with framework aluminum in the zeolite crystal. The current findings are consistent with this interpretation.

Table 5 also presents pertinent gasoline selectivity data as a function of framework and nonframework aluminum content, as defined above for the current set of catalysts. Here again, it is important to compare catalysts at or near constant conversion levels. To this end only MAT runs that fell within less than 3% of 70% conversion were used to estimate gasoline selectivity. The correlations observed between gasoline selectivity and zeolite framework and nonframework aluminum contents are depicted graphically in Figs. 7 and 8, respectively. Figure 7 reveals that the gasoline selectivity shows no correlation with the zeolite framework aluminum content. It must be noted here that the range of zeolite framework aluminum contents represented here is limited to a small fraction of the total, initial zeolite aluminum content for most samples. Furthermore, it was discussed above that the determination of framework aluminum content of steamed materials from lattice constants is subject to error at small concentrations. In contrast to framework aluminum, nonframework aluminum content shows good correlation with gasoline selectivity; see Fig. 8. According to this correlation, the gasoline selectivity decreases significantly with increasing nonframework aluminum. This

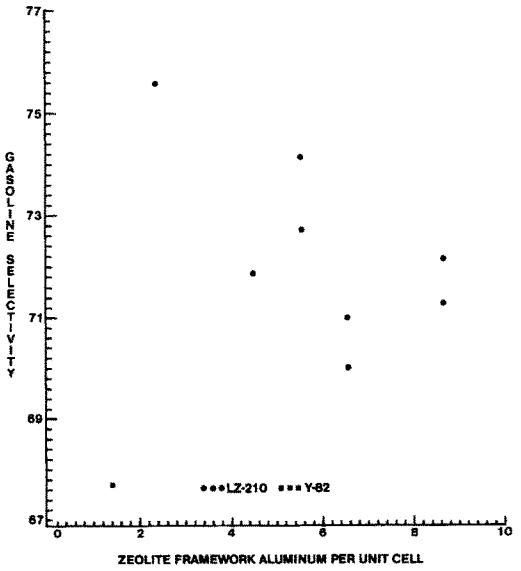

FIG. 7. Gasoline selectivity shows no correlation with zeolite framework aluminum content.

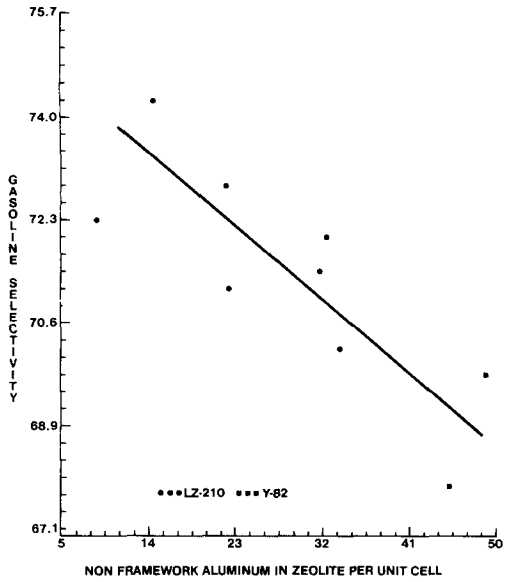

FIG. 8. The correlation of gasoline selectivity with the nonframework aluminum content of the zeolite following steam treatment.

important correlation shows that the cracking catalyzed by nonframework aluminum and by amorphous phases formed by crystal collapse is less selective to gasoline relative to the zeolitic acid sites. Thus, as the quantity of amorphous debris increases, the gasoline yield is reduced.

In summary, using severely steamed Y crystals of varying initial silica/alumina ratios it is possible to study the effect of the relatively less active, debris phase formed upon steaming. It appears that both framework and nonframework aluminum sites are catalytically active and contribute to primary cracking reactions. The two different alumina types appear to catalyze different reactions. Hydrogen transfer reactions which reduce product olefinicity and gasoline octane appear to be catalyzed only by zeolite framework acid sites, in agreement with the earlier literature report. However, some primary and particularly the secondary cracking reactions are effectively catalyzed by the nonframework alumina and amorphous silica–alumina phases formed upon steam treatment. The contribution of the latter to activity coincides with lower selectivity for primary reactions and with lower selectivity to gasoline.

Characterization of Steamed NH_4Y and LZ-210 Zeolites: Preparation and Treatment of Zeolite Samples

In order to characterize the structural and chemical effects of steaming, samples of an NH_4Y with SiO_2/Al_2O_3 ratio of 5.0 and an NH_4–LZ-210 with SiO_2/Al_2O_3 ratio of 10.2 were prepared for examination in steam-stabilized and subsequently ammonium-exchanged form, designated SN. Aliquots of both materials were further steamed in 1 atm steam at 790°C for 2 h to simulate FCC application conditions, designated SNS. The intention in choosing this steaming severity was to reduce the zeolite unit cell size to below 24.3 Å while maintaining crystallinity at a relatively high level. In order to enhance the effectiveness of the characterization techniques used here, the zeolite samples were prepared in pure zeolite powder form, without the binder or matrix components applied in the cracking studies. Therefore, it should be noted that the catalyst samples studied here were different both in composition and in steam treatment severity from those used in the cracking studies. Thus, conclusions reached by characterization of pure zeolite samples cannot be quantitatively related to the alumina-matrixed catalysts used in the MAT tests. This characterization study is mainly intended to give directional indication of processes occurring in the zeolite component of matrixed and steamed zeolite catalysts. The treatment of the samples used, the designation of the treatments, and some of the physical characteristics of the tested samples are given in Table 6. These materials were examined by solid-state NMR, electron microscopy, and Hg porosimetry. In addition, the steam-stabilized NH_4Y, SN, and its resteamed product, SNS, were further characterized by base titration for characterization of acidity.

According to the data in Table 6 the crys-

TABLE 6

Characterization of Steamed NH_4Y and LZ-210 (SiO_2/Al_2O_3 = 10.2) Samples

Treatment steps	Designation of treatment
1. Steaming at 600°C for 1 h	S
2. Ammonium exchange of product of step 1	SN
3. Steaming of product of steps 1 and 2 at 790°C for 2 h	SNS

Zeolite treatment	Surface area (m^2/g)	Unit cell size (Å)
NH_4Y, untreated	869	24.705
SNS-NH_4Y	583	24.276
LZ-210, untreated	908	24.490
SNS-LZ-210	725	24.276

tal unit cell sizes of both double-steamed SNS-NH_4Y and LZ-210 are identical even though the cell sizes of the untreated zeolites were different. This result differs from the results obtained with the alumina-matrixed catalysts used in the cracking studies. In the latter case, following steaming, the unit cell sizes of the LZ-210 zeolites were generally higher relative to similarly treated NH_4Y. Thus, the alumina matrix seems to retard the dealumination of the silicon-enriched zeolites.

According to the data in Table 6 the LZ-210 retained 83% of its original surface area after SNS treatment compared to NH_4Y which retained only 67% relative to the untreated zeolite. The smaller surface area retention of the steamed NH_4Y relative to LZ-210 reflects the superior steam stability of the silicon-enriched zeolite, in good agreement with the stability data shown in the preceding sections.

^{29}Si and ^{27}Al NMR MAS Studies of Steamed NH_4Y and LZ-210 Zeolites

^{29}Si NMR results. ^{29}Si NMR MAS spectra of the nonsteamed zeolites confirm the silicon enrichment of the LZ-210 framework relative to that of NH_4Y (see Tables 6 and 7 for the characterization of samples evaluated; Fig. 9 shows the ^{29}Si NMR MAS spectra of the NH_4Y and LZ-210 samples at all three stages of treatment). The SiO_2/Al_2O_3 ratio of the unsteamed zeolites measured from ^{29}Si NMR (*9*) (using the areas of deconvoluted peaks representing Si with 4, 3, 2, 1, and 0 aluminum next-nearest neighbors) shows some minor difference when compared to bulk SiO_2/Al_2O_3 ratio obtained from chemical analysis. The ^{29}Si NMR data are summarized in Table 8. The data for both unsteamed, starting materials are consistent with both Al and Si occupying framework cation positions. The difference between the LZ-210 framework composition determined by NMR and the bulk composition determined by chemical analysis for LZ-210 is explained by a small amount of extra-framework SiO_2 (~6.3%) indicated by an extra resonance at −110 ppm. The ^{29}Si NMR spectra show that in NH_4Y the Si(2Al) species is the most abundant, while in LZ-210 the Si(1Al) is dominant. In the LZ-210 sample the concentration of Si species with two or more Al neighbors is substantially reduced with a coincident increase in the Si(1Al) and Si(0Al) content.

Upon steaming and NH_4 exchange (SN treatment), the ^{29}Si NMR MAS spectra of both NH_4Y and LZ-210 zeolites show substantial changes in composition of the Y framework lattice. They both become aluminum depleted via framework aluminum hydrolysis. In addition, following SN treatment there is a substantial difference be-

TABLE 7

Zeolite Framework SiO_2/Al_2O_3 Ratios Calculated by ^{29}Si NMR MAS and by Chemical Analysis

Zeolite type	^{29}Si NMR MAS		Chemical analysis	
	NH_4Y	LZ-210	NH_4Y	LZ-210
1. Untreated	5.2	8.6	5.0	10.2
2. SN-treated Y[a]	8.6	17.4	5.9	12.8
3. SNS-treated Y[a]	~41	~61	5.9	12.8

[a] See Table 6 for treatment.

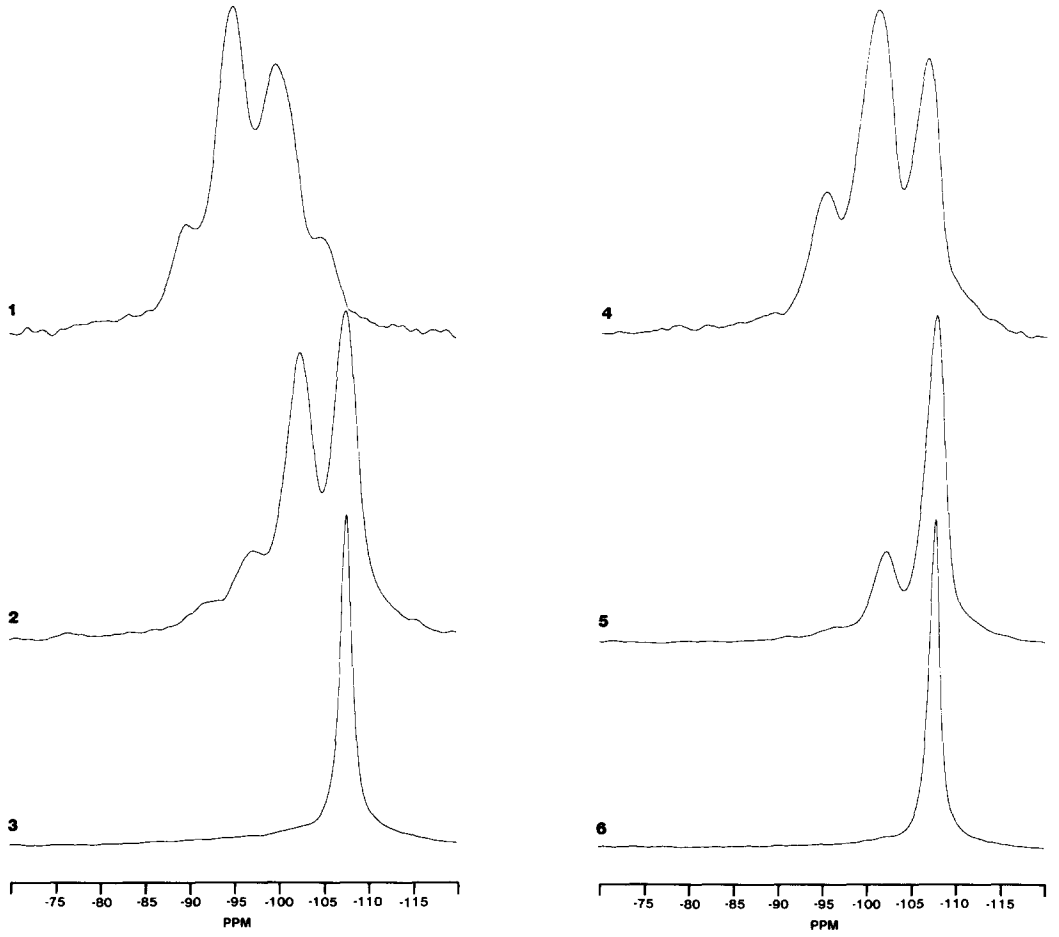

FIG. 9. ^{29}Si NMR MAS spectra. (1) NH_4Y; (2) SN-NH_4Y; (3) SNS-NH_4Y; (4) LZ-210; (5) SN-LZ-210; (6) SNS-LZ-210.

tween compositions determined by NMR and by chemical analysis. Chemical analysis is not largely affected by this treatment. However, at comparable treatments, the LZ-210 framework becomes more aluminum depleted, and thus silicon enriched, relative to the NH_4Y product according to NMR. Upon steaming and NH_4 exchange, the SN-LZ-210 retains substantially all the framework Si present in the unsteamed material as shown by the minimal formation of additional extra-framework silica (3.1%). In contrast to LZ-210, the similarly steamed SN-NH_4Y contains a significant amount (~10.4%) of nonframework silicon, not present in the untreated sample. The formation of nonframework silicon is consistent with some crystal collapse of the zeolite lattice. ^{29}Si NMR MAS spectra show that both NH_4Y and LZ-210 zeolites, first treated in steam and NH_4 exchanged, followed by a second steam treatment (designated SNS), show further depletion in framework aluminum. Again the LZ-210 SNS framework becomes somewhat more aluminum depleted relative to SNS-NH_4Y. In addition, it is notable that the framework for SNS-LZ-210 is more intact than SNS-NH_4Y. The evidence for this assertion is the amount of extra-framework Si formed from framework Si atoms. The SNS-NH_4Y contains 16.9% extra-framework Si, indicating a correspond-

TABLE 8

^{29}Si NMR Data for Dealuminated Faujasites (Deconvoluted) (7)

Sample	^{29}Si Shift δ(ppm)	Area[a]	Assignment	RMS fit
NH_4Y	−89.5	26.54	Si(3Al)	RMS
	−95.0	100.00	Si(2Al)	7.3%
	−100.2	77.49	Si(1Al)	
	−105.0	26.65	Si(0Al)	
SN-NH_4Y	−91.6	15.17	Si(3Al)	RMS
	−97.1	35.42	Si(2Al)	6.2%
	−102.5	100.00	Si(1Al)	
	−107.4	80.50	Si(0Al)	
	−110.3	26.83	Si n.f.[b]	
SNS-NH_4Y	−91.9	10.37	Si(2OH)? n.f.	
	−101.9	23.77	Si(1Al)	RMS
	−107.6	100.00	Si(0Al)	2.3%
	−112.5	14.85	Si n.f.	
LZ-210	−89.0	6.97	Si(3Al)	RMS
	−95.0	35.04	Si(2Al)	5.8%
	−100.8	100.00	Si(1Al)	
	−106.5	63.32	Si(0Al)	
	−110.9	13.72	Si n.f.	
SN-LZ-210	−91.1	1.92	Si(3Al)	RMS
	−96.6	11.16	Si(2Al)	5.1%
	−102.1	43.93	Si(1Al)	
	−105.9	17.34	?Si(0Al)	
	−107.7	100.00	Si(0Al)	
	−110.8	11.40	Si n.f.	
	−114.2	6.86	Si n.f.	
SNS-LZ-210	−94.6	2.73	Si(2Al)	RMS
	−101.9	9.18	Si(1Al)	2.5%
	−107.6	100.00	Si(0Al)	
	−112.6	7.87	Si n.f.	

[a] Relative areas with largest at 100.
[b] n.f., nonframework.

ing degree of crystal collapse while the similarly treated LZ-210 forms no new, extra-framework Si relative to the untreated sample (6.3% extra-framework Si in fresh vs 6.6% in SNS sample).

^{27}Al NMR MAS results. ^{27}Al NMR MAS spectra of the NH_4Y and LZ-210 samples have also been taken in the fresh state and following both SN and SNS treatments (see Fig. 10 for the ^{27}Al NMR MAS spectra). The interpretation of these data is more difficult because of the complexity of the spectrum and because the observable ^{27}Al NMR spectra detect only a fraction of the Al present in the samples. This was determined by taking the ^{27}Al NMR of a known amount of NH_4Y for 1000 scans and comparing the Al resonance area to that obtained for a known weight of SNS-NH_4Y obtained under the same experimental conditions, gains, and FT normalization. This experiment showed that ^{27}Al NMR could account for only 70% of the Al known to be present by chemical analysis. We conclude that 30% of the Al is present as an unsymmetrical species with linewidth too broad to

be observed by our system. Similar "undetectable" Al phases have been reported by Veeman *et al.* (*10*) for ZSM-5.

The results clearly show that the tetrahedral Al present in the framework of the untreated zeolites is gradually removed from the zeolite framework upon the SN and SNS treatments, forming an octahedral alumina phase and at least two additional new phases. One of the new phases has a position consistent with a coordination between four and six while the other is represented by a large and extremely broad background peak. The observed position of the former peak at 9.4 T is 25.9 ppm. This position compares well with the peak maximum observed and reported by Alemany and Kirker (*11*) for trigonal bipyramidal AlO_5 in andalusite. The broad component accounts for almost 75% of the Al detected in SNS-NH_4Y. The peak assigned to tetrahedral Al presumably represents the aluminum retained in the zeolite framework. A semiquantitative treatment of our ^{27}Al NMR data using the area for the deconvoluted tetrahedral resonance is consistent with residual framework Al concentrations in reasonable agreement with those calculated from the ^{29}Si NMR data. Thus our data suggest a minimum of four Al species in the SNS materials, namely, tetrahedral framework Al, intermediate (probably five-coor-

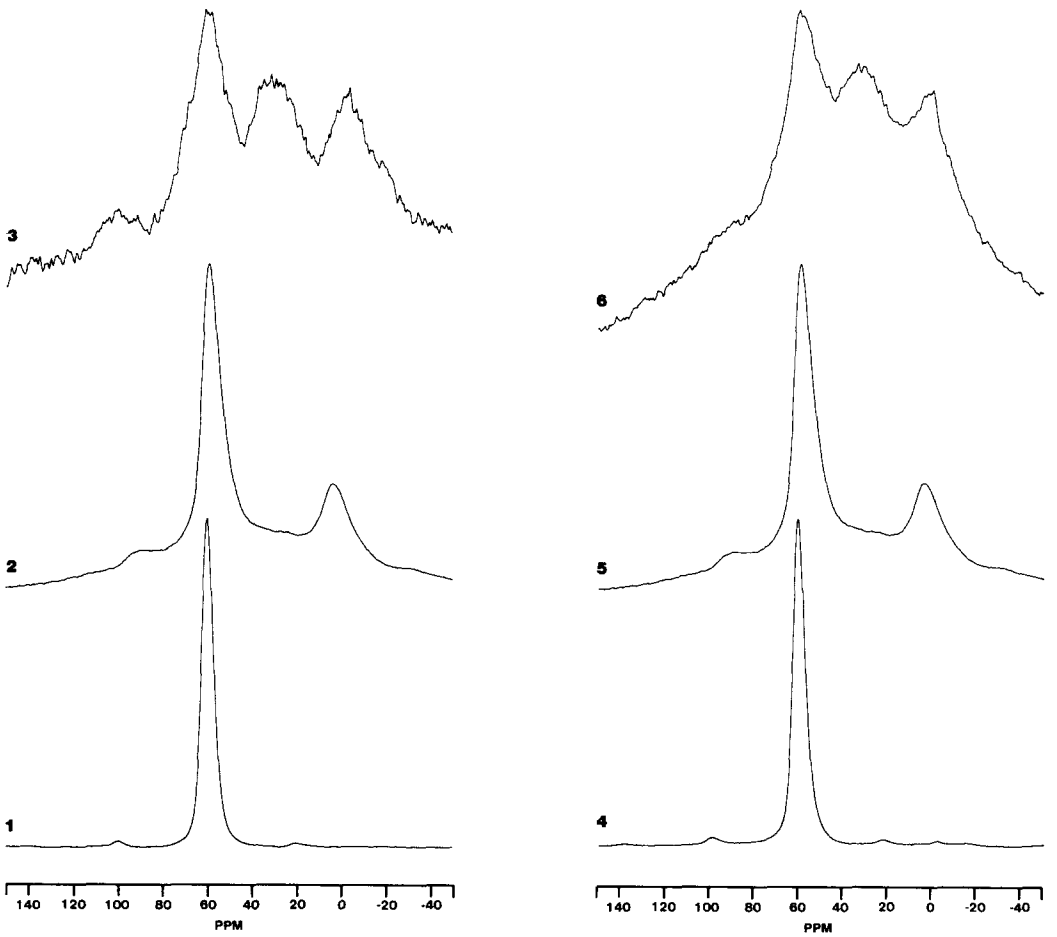

FIG. 10. ^{27}Al NMR MAS spectra. (1) NH_4Y; (2) SN-NH_4Y; (3) SNS-NH_4Y; (4) LZ-210; (5) SN-LZ-210; (6) SNS-LZ-210.

dinate–trigonal bipyramidal) Al, extra-framework octahedral Al, and a distorted geometry phase Al leading to the broad component.

Morphology of Steamed NH_4Y and NH_4–LZ-210 Zeolites

Upon hydrothermal treatment significant changes occur in the crystal structures of both NH_4Y and NH_4–LZ-210 zeolites. Following thermolysis of the NH_4^+ cations the framework alumina units react with steam and undergo hydrolysis, dehydration, and condensation steps. Gradually, depending on steaming severity, a large fraction of the original framework aluminum is removed from zeolite framework sites (*12*). Depending on the severity of steaming, one portion may form cationic oxide clusters probably occupying the sodalite cage while the fully hydrolyzed framework alumina is deposited throughout the zeolite crystal as extra-framework debris.

During steam treatment, some of the framework cation sites vacated by aluminum atoms become occupied by silicon atoms. The silicon ions migrate through the lattice, presumably aided by hydrolysis of framework oxide ions. The effect of the redistribution of framework silicon ions is to reduce the high concentration of Al vacancy sites. Ultimately, this steam-induced recrystallization results in the formation of near defect-free, silicon-rich lattice segments and intracrystalline cavities throughout the zeolite crystal. The beneficial effect of silicon migration and recrystallization is the greatly increased thermal stability of the "steam-stabilized" crystal (*12*). The recrystallization is indicated by significant narrowing of the X-ray diffraction peaks.

The secondary porosity system created by steaming represents the volume related to the aluminum and silicon removed from the crystal framework. These large pores and cavities are probably not empty since they must contain at least a fraction of the alumina and silica debris formed by removal of framework cations via hydrolysis. ESCA studies of steamed NH_4Y zeolites show only minor amounts of surface alumina outside the Y crystal. A study of the secondary pore structure formed in steamed NH_4–NaY correlated the pore size distribution with the severity of the steam treatment (*13*).

In order to compare the morphological changes occurring in double-steam-treated, SNS-NH_4Y and NH_4-LZ-210 zeolites, the steamed materials described in Table 6 were examined by electron microscopy and by Hg porosimetry. Electron microscopy of sectioned single crystals of unsteamed samples shows a smooth surface, free of any observable defect. In contrast, both SNS-treated samples display uneven surfaces, decorated with cavities of varying sizes throughout the whole zeolite matrix. Cavities of ~50–200 Å diameter are frequent but larger cavities are also present.

The Hg porosimetries of the fresh and SNS-NH_4Y and SNS-LZ-210 samples are shown in Fig. 11. The curves show that in SNS-NH_4Y the secondary pores accessible to Hg range from ~30 to ~1,500 Å occupying about 12 vol% of the crystal. The secondary pores accessible to Hg in the SNS-

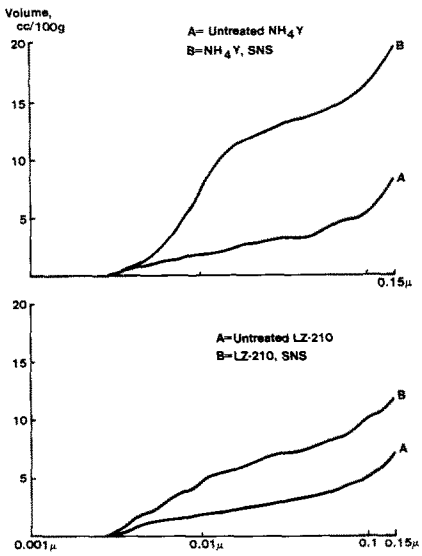

FIG. 11. Pore volume distribution for NH_4Y, SNS-NH_4Y, LZ-210, and SNS-LZ-210.

LZ-210 sample occupy only 5 vol%. It is apparent from the curves that the SNS-NH_4Y has substantially more accessible pores between 70 and 180 Å in size relative to SNS-LZ-210.

Characterization of Steam-Treated NH_4Y and LZ-210 Zeolites by Thermometric Titration

While the acid sites in zeolites have been characterized by numerous investigators using a variety of spectroscopic, ion exchange, sorption, and titration techniques, no fully satisfactory technique emerged as yet to provide information fully consistent with catalytic data. Therefore, most frequently, hydrocarbon reactions proceeding via carbocations are chosen to characterize zeolite acid strength. While these experiments give reliable and practical information for large-pore zeolites on catalytic activity and, thus, on effective acidity, they provide no information on the range of intrinsic acid strength and on acid site distribution.

In this study we have chosen thermometric titration to characterize the distribution of acid sites of steam-treated NH_4Y zeolites, including the SN and SNS materials, using pretreatments described in Table 6. The thermometric titration method chosen here was earlier described by Bezman (*14*). Using this method the titration is carried out with *n*-butylamine in the presence of benzene. Benzene is used to facilitate equilibration of the base among zeolite acid sites. The method was claimed to be quite satisfactory for Y zeolites but it was found ineffective with mordenite. In the latter case the one-dimensional pores presumably became plugged by the strongly adsorbed *n*-butylamine, preventing equilibration of the base among acid sites. With acidic Y zeolites, however, the full titer corresponding to calculated protonic acidity was readily achieved. In fact titers, exceeding full protonic acidity, calculated from cation exchange capacity, have also been measured with steam-stabilized Y. The "excess" titer

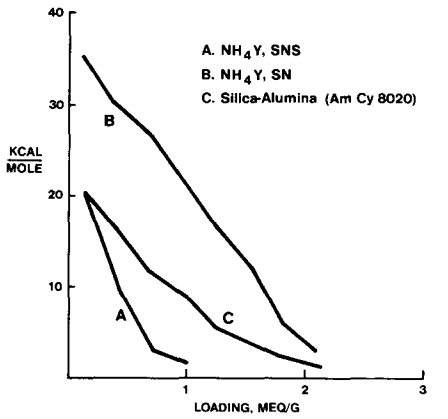

FIG. 12. Thermometric titration of the acid sites distribution for steam-treated Y zeolite and amorphous silica–aluminum.

was ascribed to interaction of the base with Lewis acid sites (*14*).

The *n*-butylamine titration technique described above was used to compare the acid titer of the steam-stabilized and NH_4^+-exchanged NH_4Y, SN, with its resteamed product, SNS; see Fig. 12. The figure shows that the steam-stabilized Y (SN) has acid sites of widely ranging acidity, including very strong acid sites represented by ~35 kcal/mol heat of interaction with the base; see curve B in Fig. 12. In contrast, the severely resteamed SNS product shows no acid sites with more than 20 kcal/mol interaction with the base. In addition, the amount of acid sites in the latter material are reduced by about a factor of 2 relative to the SN material. For comparison, the titration curve of a commercial silica–alumina gel catalyst (American Cyanamid 8020) has also been taken using the same technique; see curve C in Fig. 12. The similarity between the SNS-Y zeolite and that of the amorphous silica–alumina gel catalyst is apparent; they both represent the same range of weak to medium acid strength. Interestingly, the *n*-butylamine titers of the SN-NH_4Y and the silica–alumina gel are about the same while the titer of the SNS-Y product is only one-half relative to the two other materials. This amount

is similar to the amount of alumina-containing amorphous debris formed upon steaming.

It must be noted here that the thermometric titration experiment is particularly delicate at the beginning of the measurement, and initial values representing small concentrations of strongest acid sites can be easily missed in the measurement. Therefore, we assume that in the SNS zeolite sample the minor amount of strong acid sites associated with residual framework aluminum, indicated by both ^{27}Al NMR and X-ray a_0 measurements, were present but not recorded at the start of the titration experiment.

The *n*-butylamine titration data are consistent with the interpretation that the twice-steamed SNS-NH_4Y zeolite product contains an acidic debris which in acid strength closely resembles that of a silica–alumina gel. Its quantity is estimated to be about one-half relative to the acid sites present in the steam-stabilized NH_4Y.

CONCLUSIONS

Catalytic cracking studies and physicochemical characterization of steamed NH_4Y and LZ-210 zeolite catalysts provide consistent information about the chemical and structural processes occurring in zeolite crystals in the FCC process. They also show important differences in both chemical and structural characteristics and catalytic properties between NH_4Y and LZ-210 zeolites.

The severe steaming encountered in FCC process causes gradual dealumination of the Y crystal lattice, ultimately resulting in the removal of most of the aluminum from the framework. Along with the formation of the nonframework alumina phase a secondary, macropore system is formed throughout the zeolite crystal. Parallel with this process a gradual crystal loss is observed which increases at higher temperatures and higher steaming severities. The amorphous phases formed upon steaming display an intrinsic acid strength and acid site concentration similar to those of amorphous silica–alumina gel.

The catalytic properties of the zeolite acid and the acid sites associated with the amorphous phases are different. The zeolite acid has much higher activity for cracking and for hydride transfer reactions, and it has higher gasoline selectivity relative to the amorphous phases formed upon steaming. The amorphous phases contribute to both primary and secondary cracking, the latter causing increased gas formation and lower gasoline yields.

The silicon-enriched LZ-210 zeolites are more stable to steaming relative to steam-stabilized NH_4Y. Their crystal retention is greater at higher silicon contents. According to NMR data, upon steaming, the silicon-enriched zeolites maintain framework silicon content and crystallinity to a larger extent relative to NH_4Y. Therefore, following comparable treatments, LZ-210 zeolites retain higher crystallinity, and they contain smaller amounts of amorphous acid debris relative to NH_4Y. With a higher contribution from the zeolite acid relative to the amorphous acid debris, they display superior activity retention and gasoline selectivity relative to similarly treated NH_4Y.

ACKNOWLEDGMENTS

The authors express their appreciation to Mr. A. P. Risch for his contribution in the early catalyst synthesis and testing, to Mr. Al Springer for the preparation of the zeolite samples, to Mr. Mark Staniulis for carrying out the thermometric titrations, and to Mr. Herb Hillery and Dr. Kathy Reuter for conducting the electron microscopy studies.

REFERENCES

1. Skeels, G. W., and Breck, D. W., "Proceedings, Sixth Int. Zeolite Conf.," pp. 87–96, 1984.
2. Rabo, J. A., *et al.*, "Proceedings, 1986 NPRA Annual Meeting," AM-86-30.
3. Long, G. N., *et al.*, "Katalistiks Seventh Annual Fluid Cat Cracking, Venice, Italy, May 12–13, 1986."
4. Pine, L. A., *et al.*, *J. Catal.* **85,** 466 (1984).
5. ASTM Method D-3907.
6. Derouane, E. G., *et al.*, *J. Catal.* **63,** 331 (1980).
7. Breck, D. W., and Flanigen, E. M., "Molecular Sieve," p. 47. Society of the Chemical Industry, London, 1968.

8. Lunsford, *et al.*, *Zeolites* **6,** 225 (1986).
9. Bennet, J. M., Blackwell, C. S., and Cox, D. E., *J. Phys. Chem.* **87,** 3783 (1983).
10. Geurts, F. M. M., Kentgens, A. P. M., and Veeman, W. S., *Chem. Phys. Lett.* **120**(2), 206 (1985).
11. Alemany, L. B., and Kirker, G. W., *J. Amer. Chem. Soc.* **108,** 6158 (1986).
12. Breck, D. W., and Skeels, G. W., *ACS Symp. Ser.* **40,** 23 (1977).
13. Zukal, A., *et al.*, *Zeolites* **6,** 133 (1986).
14. Bezman, R., *J. Catal.* **68,** 242 (1981).